

Investigation of Anti-SOD1 Antibodies Yields New Structural Insight into SOD1 Misfolding and Surprising Behavior of the Antibodies Themselves

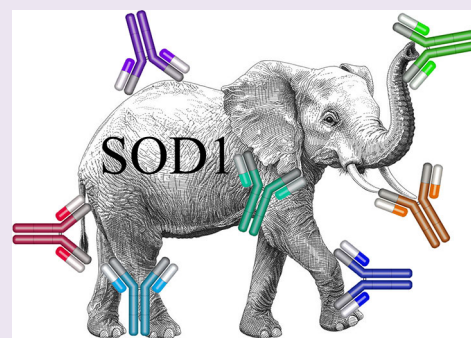
Ryan S. Atlasi,[†] Ravinder Malik,[†] Christian I. Corrales,[†] Laura Tzeplaef,† Julian P. Whitelegge,^{‡,§,||} Neil R. Cashman,[⊥] and Gal Bitan^{*,†,§,||}

[†]Department of Neurology, [‡]Department of Psychiatry and Biobehavioral Sciences, David Geffen School of Medicine, [§]Brain Research Institute, and ^{||}Molecular Biology Institute, University of California, Los Angeles, Los Angeles, California 90095, United States

[⊥]Department of Neurology, University of British Columbia (UBC), Vancouver, British Columbia V6T 2B5, Canada

Supporting Information

ABSTRACT: Mutations in Cu/Zn-superoxide dismutase (SOD1) gene are linked to 10–20% of familial amyotrophic lateral sclerosis (fALS) cases. The mutations cause misfolding and self-assembly of SOD1 into toxic oligomers and aggregates, resulting in motor neuron degeneration. The molecular mechanisms underlying SOD1 aggregation and toxicity are unclear. Characterization of misfolded SOD1 is particularly challenging because of its metastable nature. Antibodies against misfolded SOD1 are useful tools for this purpose, provided their specificity and selectivity are well-characterized. Here, we characterized three recently introduced antimisfolded SOD1 antibodies and compared them with two commercial, antimisfolded SOD1 antibodies raised against the fALS-linked variant G93A-SOD1. As controls, we compared the reactivity of these antibodies to two polyclonal anti-SOD1 antibodies expected to be insensitive to misfolding. We asked to what extent the antibodies could distinguish between WT and variant SOD1 and between native and misfolded conformations. WT, G93A-SOD1, or E100K-SOD1 were incubated under aggregation-promoting conditions and monitored using thioflavin-T fluorescence, electron microscopy, and dot blots. WT and G93A-SOD1 also were analyzed using native-PAGE/Western blot. The new antimisfolded SOD1 and the commercial antibody B8H10 showed variable reactivity using dot blots but generally showed maximum reactivity at the time misfolded SOD1 oligomers were expected to be most abundant. In contrast, only B8H10 and the control antibodies were reactive in Western blots. Unexpectedly, the polyclonal antibodies showed strong preference for the misfolded form of G93A-SOD1 in dot blots. Surprisingly, antimisfolded SOD1 antibody C4F6 was specific for the apo form of G93A-SOD1 but insensitive to misfolding. Antibody 10C12 showed preference for early misfolded structures, whereas 3H1 bound preferentially to late structures. These new antibodies allow distinction between putative early- and late-forming prefibrillar SOD1 oligomers.



ALS is a progressive neurodegenerative disease that causes death of motor neurons. In most cases, the life expectancy for patients with ALS is 3–5 years after diagnosis.¹ Approximately 10% of ALS cases are familial, and of those, 10–20% are associated with >180 mutations in the Cu/Zn Superoxide Dismutase (SOD1) cognate gene (<http://alsod.iop.kcl.ac.uk>). SOD1 is a homodimeric, antioxidant enzyme that catalyzes highly reactive superoxide radical anions formed during respiration into less reactive hydrogen peroxide. Each monomer complexes one Cu²⁺ and one Zn²⁺ ion, which are essential for the structural stability and catalytic activity of SOD1,² and contains a highly conserved intramolecular disulfide bond. Reduction of the disulfide bond and/or loss of the metal ions destabilize the structure of SOD1, leading to its misfolding and self-assembly into toxic oligomers and aggregates.^{3,4}

Multiple studies have characterized the aggregation mechanism, kinetics, and fibril morphology of SOD1,^{5–7} whereas

characterization of SOD1 oligomers has been more challenging because of their metastable nature. The oligomers are short-lived, exist in dynamically changing mixtures, and their structures are influenced by the method of preparation. Antibodies specific for the oligomeric and misfolded structures of amyloidogenic proteins are useful tools for identifying these structures in biological samples,^{8–10} though they should be used with caution because of potential low specificity and cross-reactivity.^{11,12} Antibodies against misfolded SOD1 have been prepared taking advantage of knowledge of the three-dimensional structure of the dimeric protein and using epitopes buried in the dimer interface.¹³ However, information about the specificity of many antibodies is limited and, in many cases, the

Received: August 7, 2018

Accepted: August 15, 2018

Published: August 15, 2018

Table 1. List of Investigated Anti-SOD1 Antibodies and Their Expected Specificities

antibody	raised in	antigen	type	expected reactivity/specificity
Ab16831 (Abcam)	rabbit	total human WT SOD1	pAb ^a	total SOD1
2770 (Cell Signaling Technology)	rabbit	human SOD1 N-terminal epitope	pAb	total SOD1
B8H10 (MédiMabs)	mouse	human G93A SOD1	mAb ^a	misfolded SOD1
C4F6 (MédiMabs)	mouse	human G93A SOD1	mAb	misfolded SOD1
AMF7-63	rabbit	the electrostatic loop D ¹²⁵ DLGKGGNEESTKTGNAG ¹⁴²	mAb	high affinity for misfolded SOD1
3H1	mouse	the electrostatic loop D ¹²⁵ DLGKGGNEESTKTGNAG ¹⁴²	mAb	1000-fold lower affinity than AMF7-63
10C12	mouse	SOD1-exposed dimer interface (SEDI) ¹³ with Cys146 replaced by cysteic acid	mAb	oxidized misfolded SOD1 monomers/oligomers/aggregates

^amAb = monoclonal antibody. pAb = polyclonal antibody.

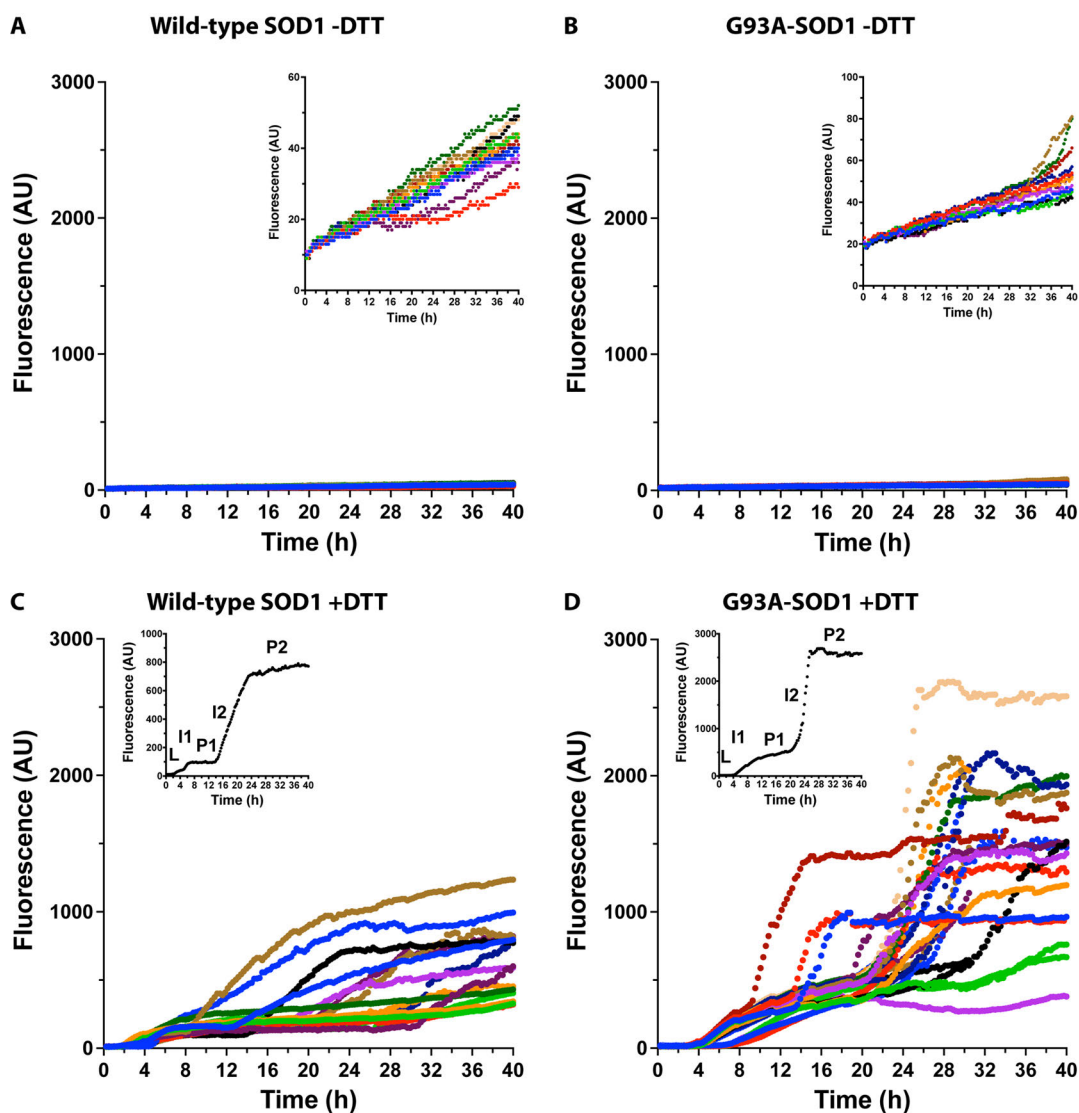


Figure 1. Temporal change in β -sheet content of WT or G93A-SOD1 measured using ThT fluorescence. 40 μ M of WT (A, C) or G93A- (B, D) SOD1 were incubated at 37 $^{\circ}$ C with fast agitation in the absence (A, B) or presence (C, D) of 25 mM DTT and the change in ThT fluorescence was monitored in a plate reader for 40 h. To facilitate comparison, all the reactions are shown with the same scale in the y-axis. In panels A and B, the insets show the small changes in fluorescence using adjusted y-axis scales. In panels C and D, insets show one reaction with the lag phase (L), first small increase (I1), first plateau (P1), second large increase (I2), and final plateau (P2) indicated.

exact epitope and binding characteristics are not validated. Unreliability and insufficiently characterized antibodies have been a major impediment for data reproducibility in biomedical research, including ALS research.^{14–16}

To address these issues, here, we characterized three new antimisfolded-SOD1 antibodies¹⁷ and compared them with two commercial, antimisfolded-SOD1 antibodies raised against the fALS-linked variant G93A-SOD1. We compared the reactivity of these antibodies to two polyclonal anti-SOD1 antibodies that

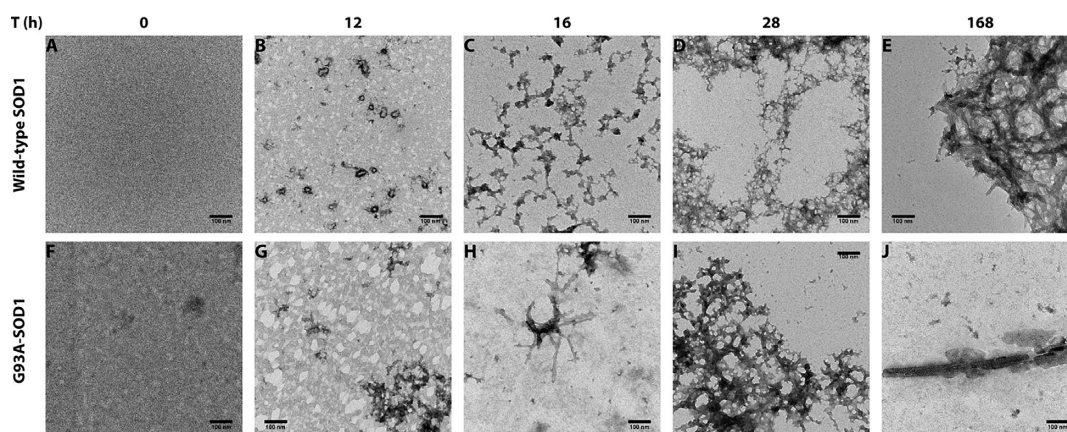


Figure 2. Morphological changes in WT and G93A-SOD1 during incubation. Aliquots from aggregation reactions were taken for morphological examination by EM. Representative images are shown for the WT and G93A-SOD1 isoforms. The scale bars denote 100 μm .

were expected to be insensitive to misfolding (Table 1). We investigated whether the antibodies could distinguish among native and misfolded forms of SOD1 and how their binding was affected by SOD1 self-assembly. Interestingly, the results revealed that the behavior of several antibodies did not match their expected reactivity. In addition, the different temporal change in antibody reactivity relative to the increase in thioflavin T (ThT) fluorescence showed formation of early and late SOD1 structures, presumably oligomers, which to our knowledge, have not been reported previously.

RESULTS AND DISCUSSION

SOD1 Aggregation Is Highly Variable and Includes Two Distinct Structural Change Steps. To create a baseline to which characterization of anti-SOD1 antibodies could be related, the aggregation process first was monitored for 40 h using the ThT fluorescence assay, which measures formation of the typical cross- β structure of amyloids.¹⁸ To facilitate the reaction, we used the demetalated, apo form of WT or G93A-SOD1 and induced the aggregation by addition of 25 mM DTT.⁵ In control reactions, apo-SOD1 was incubated under identical conditions in the absence of DTT. Because the kinetics of unseeded SOD1 aggregation has been reported to be highly variable,^{19–21} multiple reactions were monitored in parallel in 96-well plates using a plate reader.

As expected, under nonreducing conditions, the ThT fluorescence signal for WT or G93A-SOD1 showed little change during the 40-h incubation (Figure 1A,B), suggesting minimal misfolding and aggregation. In contrast, in the presence of DTT (Figure 1C,D), in all of the reactions we observed a substantial increase in the ThT fluorescence signal, consistent with misfolding and formation of β -sheet-rich amyloid. This behavior was more prominent in G93A-SOD1 (Figure 1D) than in WT SOD1 (Figure 1C), in agreement with the increased tendency of G93A-SOD1 to aggregate. Interestingly, inspection of the ThT curves revealed a two-phase process in most cases (Figure 1C,D insets). After an initial lag phase (L), the ThT fluorescence showed a small increase (I1) followed by an intermediary plateau or “pause” (P1). Then, a second, large increase in ThT fluorescence (I2) was observed, culminating in a final plateau (P2). A similar behavior has been observed previously in aggregation reactions of N139D-SOD1 and the triply substituted variant N26D/N131D/N139D-SOD1.²² Another study measuring the aggregation kinetics of WT SOD1 in the presence of small peptides with high aggregation propensity

derived from the sequence of WT SOD1 showed similar, two-step ThT curves, but only in the presence of the peptide inducers.⁷ To our knowledge, our study is the first one to observe this behavior for WT SOD1 itself or for G93A-SOD1. A possible explanation for this unusual behavior was the high speed of agitation of the samples, which was imposed by the available settings of the plate reader used in our experiments, a BioTek Synergy HT, in which the slowest agitation setting is 1020 rpm. To test if this was the case, we performed similar reactions in a newer model, BioTek Synergy HTX, at an agitation speed of 300 rpm. Under these conditions, we did not observe an increase in ThT fluorescence during the same incubation time. However, when we added Teflon balls to the wells, which were not included in the reactions performed in the older instrument, the ThT fluorescence did increase, and in some reactions, we observed a two-step profile (Supplementary Figure 1), similar to the one shown in Figure 1C,D, suggesting that this behavior was an intrinsic feature of SOD1 aggregation and not restricted to a particular experimental setting. Presumably, under the conditions we used, the misfolding of native SOD1 and subsequent nucleation step were accelerated, but elongation initially was suppressed leading to a “pause” in the reaction and observation of the intermediate plateau phase, P1. However, the exact mechanism controlling the two-step kinetic profile is not clear and will require further study.

Examining the behavior of different replicates, it was evident that the length of the different steps varied substantially. An exception was the initial lag phase, which was fairly consistent among different replicates and was shorter for WT SOD1 (~ 1.5 h) than for G93A-SOD1 (~ 4 h) (cf. Figure 1C,D). This trend was reversed in the experiments shown in Supplementary Figure S1, which were done later, further demonstrating the stochastic nature of the process. A literature search showed that lag times of fALS-related SOD1 variants that were longer than that of WT SOD1 have been reported previously.^{23,24} The differences may be related to small variations in experimental conditions and possibly residual metal-ion content of the proteins. The fluorescence values and duration of the other steps of the ThT curves were highly variable. For example, the final plateau values were in the range 200–1250 for WT SOD1 and 370–2600 for G93A-SOD1. Nearly 30% of the WT SOD1 aggregation reactions reached the final plateau, whereas >90% of the G93A-SOD1 aggregation reactions reached the final plateau, demonstrating the accelerated aggregation of the latter (Figure 1C,D).

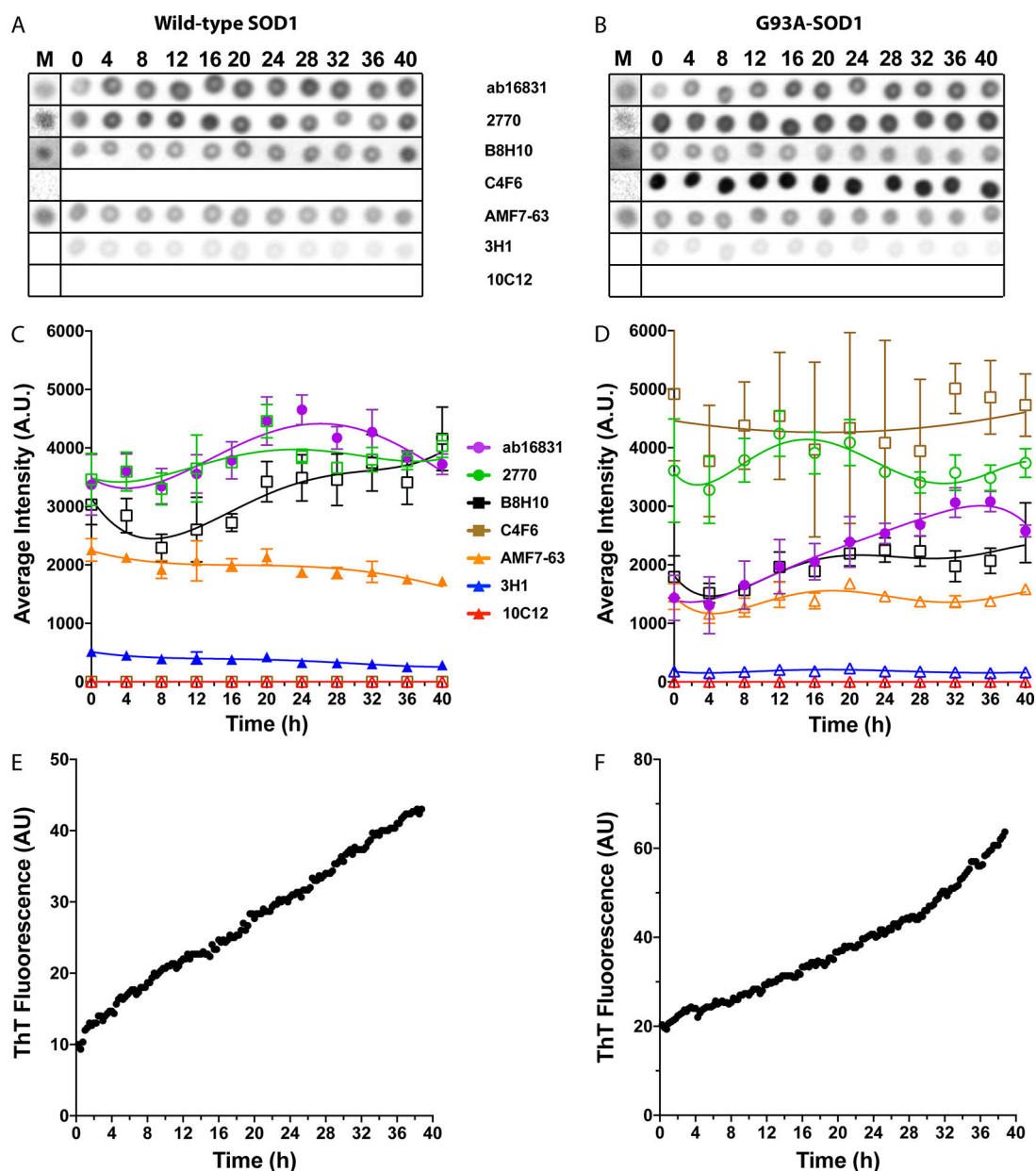


Figure 3. Antibody reactivity for WT and G93A-SOD1 under nonreducing conditions. Aliquots from the same aggregation reactions shown in Figure 1 were taken every 4 h and dot-blotted on nitrocellulose membranes. At the end of the experiment, each membrane was blocked and then probed, stripped, and reprobbed with the seven antibodies. The order of the antibodies was changed in different replicates to avoid bias due to loss of protein during strip and reprobe cycles. (A,B) Representative dot blots of the apo forms of WT (A) and G93A- (B) SOD1 incubated under nonreducing conditions at different time points. The metalated form of each protein is shown on the left (indicated by M) as a control. (C,D) Averaged densitometric analysis of two independent experiments, each with six replicates ($n = 12$) of WT (C) and G93A- (D) SOD1. The lines are added to help guide the eye but do not imply that the points should be connected. Filled symbols represent cases in which the change in antibody binding during the reaction was found to be statistically significant, whereas empty symbols represent insignificant changes (one-way ANOVA). (E,F) Representative ThT fluorescence curves from the same reactions of WT (E) and G93A- (F) SOD1.

SOD1 Forms a Mixture of Amorphous and Fibrillar Assemblies. To examine the correlation between the aggregation kinetics and morphology of SOD1, separate aggregation reactions were conducted as described in the Methods. Aliquots of these reaction mixtures were taken at different time points during the aggregation reaction and were used to measure ThT fluorescence (not shown) and in parallel for morphological examination by EM (Figure 2). Initially, ($t = 0$ h), no protein was observed, suggesting that only SOD1 monomers or dimers, which are too small to be observed under the conditions used, were present (Figure 2A,F). At 12 h,

corresponding in most cases to the P1 phase observed in ThT experiments, small ring-like aggregates were observed in the WT protein (Figure 2B), whereas G93A-SOD1 formed amorphous structures (Figure 2G). At $t = 16$ h, a later time point during the P1 phase in most reactions, the morphology of WT SOD1 changed to small amorphous aggregates connected by thread-like structures (Figure 2C). Similar morphologies also were observed for G93A-SOD1, in addition to short fibrils (Figure 2H). At 28 h, during a period in which most reactions reached the final plateau, P2, a large mesh of amorphous threads, which were thinner in WT SOD1 and thicker in G93A-SOD1, was

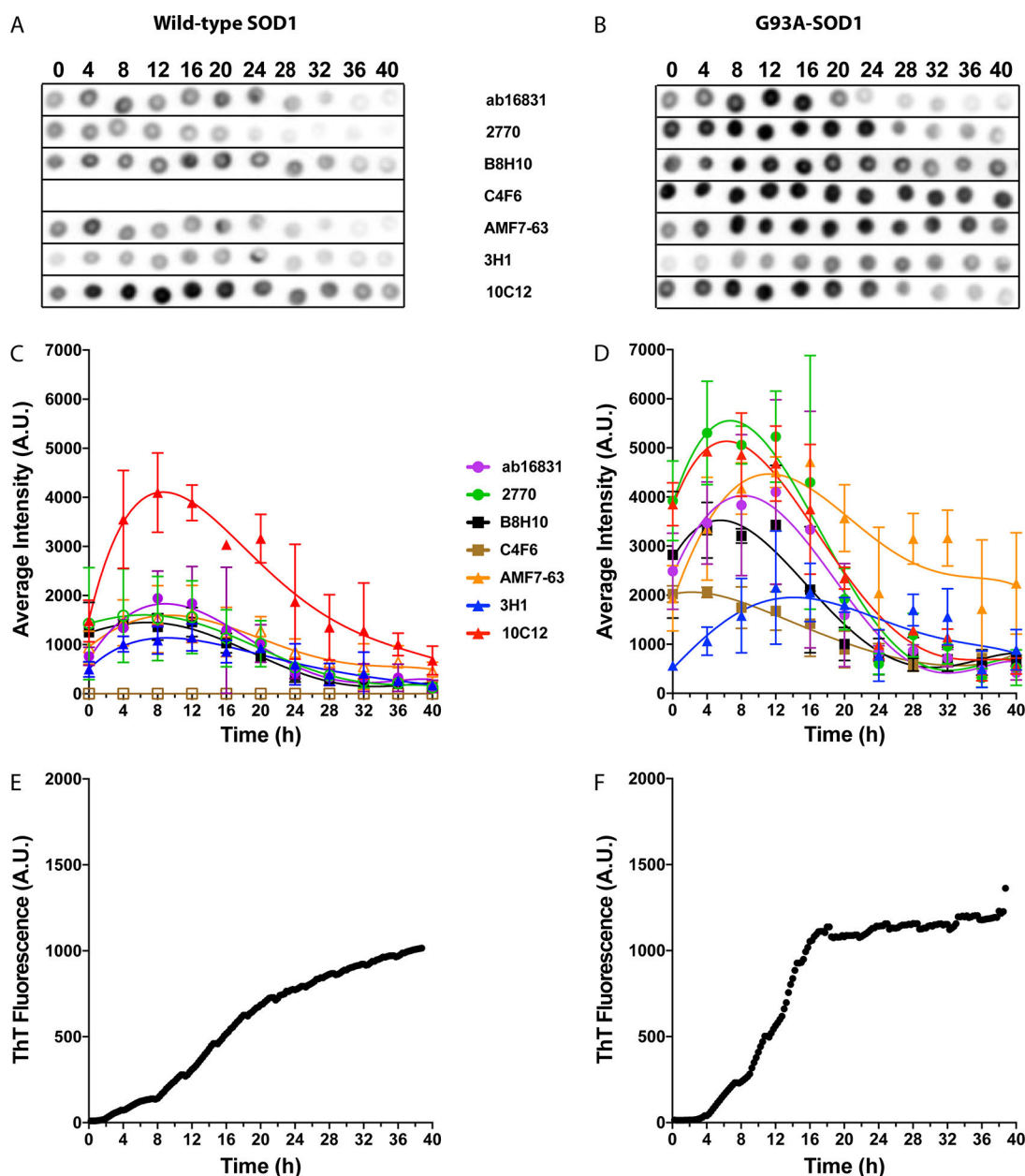


Figure 4. Antibody reactivity for WT and G93A-SOD1 under reducing conditions in reactions with short “pause” (P1) periods. Aliquots from the same aggregation reactions shown in Figure 1 were taken every 4 h and dot-blotted on nitrocellulose membranes. At the end of the experiment, each membrane was blocked and then probed, stripped, and re-probed with the seven different antibodies. The order of the antibodies was changed in different experiments to avoid bias due to loss of protein during strip and reprobe cycles. (A,B) Representative dot blots of WT (A) and G93A- (B) SOD1 reactions in which the initial plateau phase, P1, was relatively short, i.e., ≤ 10 h for WT SOD1 and ≤ 7 h for G93A-SOD1, incubated under reducing conditions at different time points. (C,D) Averaged values from densitometric analysis of two independent experiments, including a total of nine replicates of WT (C) and six replicates of G93A- (D) SOD1. The lines are added to help guide the eye but do not imply that the points should be connected. Filled symbols represent cases in which the change in antibody binding during the reaction was found to be statistically significant, whereas empty symbols represent insignificant changes (one-way ANOVA). (E,F) Representative ThT fluorescence curves from the same reactions of WT (E) and G93A- (F) SOD1.

observed (Figure 2D,I), in addition to occasional fibrils. Finally, at ~ 168 h (1 week), large amorphous aggregates and occasional fibrils integrated within them were observed (Figure 2E,J). Overall, the majority of the morphologies observed were amorphous, rather than fibrillar, despite the high ThT signal, suggesting that under the conditions used here, SOD1 largely was arranged in β -sheets, but the structures were not classical amyloid.

Characterization of Conformational Changes during SOD1 Aggregation Using Dot Blots with Anti-SOD1 Antibodies. To set a baseline for antibody reactivity, we analyzed first the behavior of the antibodies with WT- and G93A-SOD1 incubated in the absence of DTT. Under these conditions, we expected SOD1 to maintain primarily a native-like dimeric structure, an expectation supported by the minimal change in ThT fluorescence observed during the experiment (Figure 1A,B and Figure 3E,F). Thus, we predicted that under

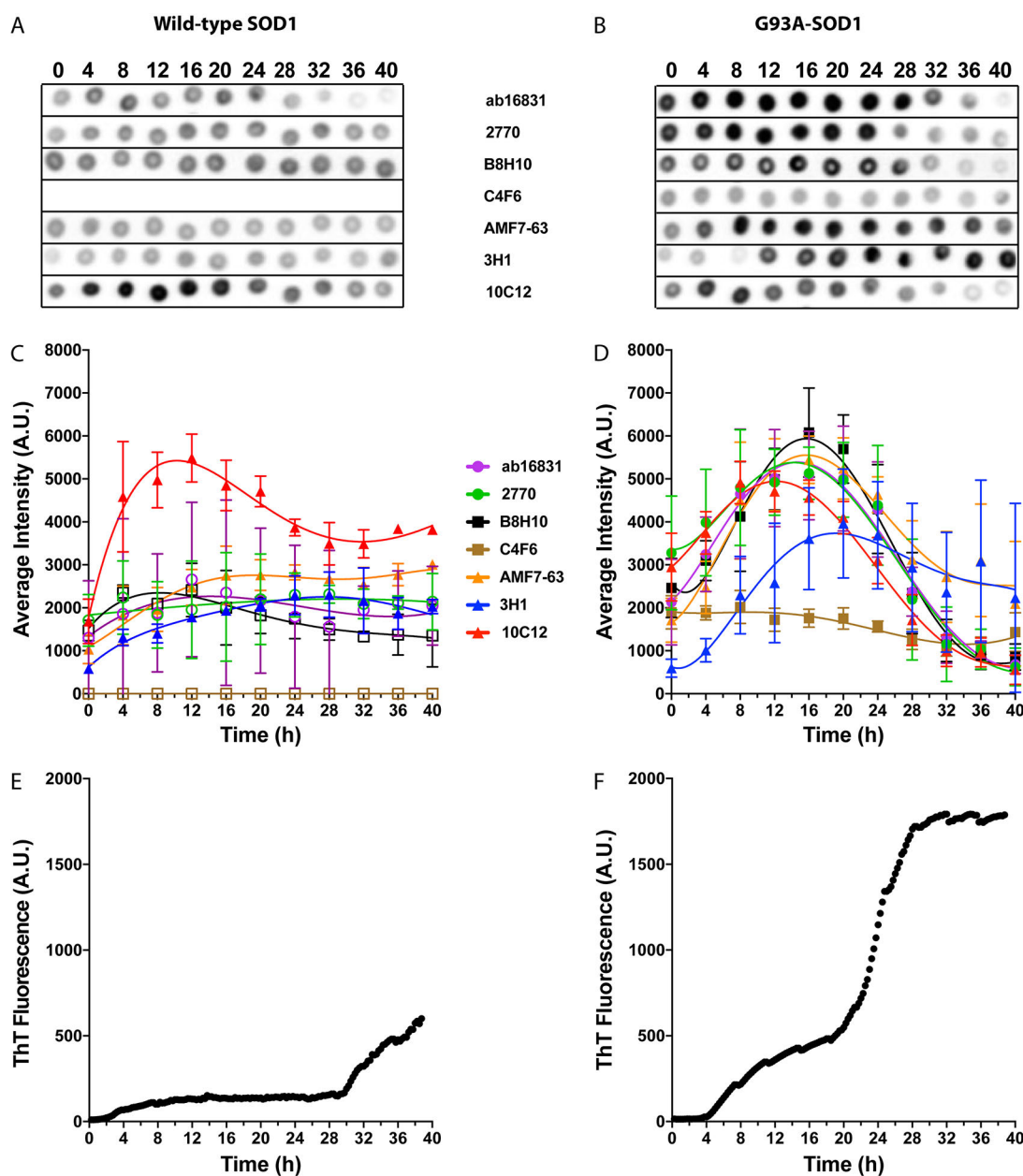


Figure 5. Antibody reactivity for WT and G93A-SOD1 under reducing conditions in reactions with long “pause” (P1) periods. Aliquots from the same aggregation reactions shown in Figure 1 were taken every 4 h and dot-blotted on nitrocellulose membranes. At the end of the experiment, each membrane was blocked and then probed, stripped, and reprobbed with the seven different antibodies. The order of the antibodies was changed in different experiments to avoid bias due to loss of protein during strip and reprobe cycles. (A,B) Representative dot blots of WT (A) and G93A- (B) SOD1 reactions in which the initial plateau phase, P1, was relatively long, i.e., >10 h for WT SOD1 and >7 h for G93A-SOD1, incubated under reducing conditions at different time points. (C,D) Averaged values from densitometric analysis of two independent experiments, including a total of three replicates of WT (C) and six replicates of G93A- (D) SOD1. The lines are added to help guide the eye but do not imply that the points should be connected. Filled symbols represent cases in which the change in antibody binding during the reaction was found to be statistically significant, whereas empty symbols represent insignificant changes (one-way ANOVA). (E,F) Representative ThT fluorescence curves from the same reactions of WT (E) and G93A- (F) SOD1.

these conditions only the antibodies that were not specific for misfolded SOD1, Ab16831, and 2770^{17,25,26} would bind to SOD1.

To characterize the antibody binding to SOD1, aliquots of the reaction mixtures were taken every 4 h during the same aggregation reactions used for ThT fluorescence monitoring, and deposited onto nitrocellulose membranes for dot-blot analysis. The membranes then were probed with each of the seven antibodies, the dots were quantified densitometrically, and

the reactivity of each antibody was plotted against time. To avoid a systematic error due to potential gradual loss of material with multiple strip/reprobe cycles, the order of the antibodies was changed for different membranes. In separate experiments, the metalated version of each SOD1 variant was probed as a control.

The two pAbs, Ab16831 and 2770, indeed showed high reactivity with both WT (Figure 3A,C, here, and in all subsequent figures, the lines are meant to help guide the eye, not to suggest that the dots should be connected) and G93A-

SOD1 (Figure 3B,D). They showed approximately the same reactivity with WT SOD1, whereas the reactivity of 2770 with G93A-SOD1 was significantly higher than that of Ab16831 ($p < 0.0001$, 2-way ANOVA). Interestingly, this high reactivity of 2770 with G93A-SOD1 was only with the apo form, whereas low reactivity was observed with the metalated form (Figure 3B). There was no difference between the reactivity of 2770 with the metalated and apo forms of WT SOD1, or between the reactivity of Ab16831 with the apo and metalated forms of either SOD1 isoform.

Surprisingly, the antimisfolded SOD1 mAbs B8H10^{27–29} and AMF7-63²⁸ also bound to both isoforms of SOD1 under nonreducing conditions, regardless of metalation (Figure 3A–D). Previously, it has been suggested that filter binding might partially denature SOD1, potentially inducing exposure of the disordered electrostatic loop recognized by the high-affinity antibody AMF7-63, but not by the lower-affinity mAb 3H1, which was raised against the same antigen. In support of this interpretation, AMF7-63 was reported not to bind to spinal cord sections of transgenic mice expressing human, WT SOD1.²⁸

As expected, mAb 3H1^{17,30} showed very weak binding to the apo form of WT or G93A-SOD1 and no binding to the metalated form. mAb 10C12^{17,30} did not bind at all to either SOD1 isoform regardless of metalation. Interestingly, C4F6, which was expected to bind only misfolded SOD1^{29,31,32} did not bind at all to WT SOD1 (Figure 3A,C) or to metalated G93A-SOD1, but had the highest apparent reactivity for apoG93A-SOD1 (Figure 3B,D), suggesting that it is specific for apoG93A-SOD1 and not for misfolded SOD1. As expected, under the nonreducing conditions used in these experiments, most of the antibodies bound to both WT and G93A-SOD1 with little change in apparent reactivity during the incubation. To determine whether a change in reactivity occurred, we used a one-way ANOVA to calculate whether the reactivity at each time point differed significantly from the initial or final time points. The antibodies for which a significant change was found are shown in filled symbols, whereas those that showed no significant change are shown in empty symbols (Figure 3C,D; 4C,D; and 5C,D). The analysis showed that the reactivity of Ab16831 increased significantly and then decreased during the incubation of both SOD1 isoforms, and that the reactivity of both AMF7-63 and 3H1 decreased during the incubation of WT SOD1. However, these changes were relatively small in magnitude and may reflect experimental variability.

We also compared the reactivity of the antibodies to each other using a 2-way ANOVA. The analysis showed that the antibodies could be divided into groups, with significant differences among the groups, and little or insignificant differences within each group. In the case of WT SOD1, a low-reactivity group consisted of C4F6, 3H1, and 10C12. AMF7-63 showed medium reactivity, whereas a high-reactivity group comprised Ab16831, 2770, and B8H10. In the case of G93A-SOD1, mAbs 3H1 and 10C12 were in the low-reactivity group, whereas C4F6 moved to the high-reactivity group, together with pAb 2770. Ab16831, B8H10, and AMF7-63 comprised the medium-reactivity group.

Next, we asked whether the reactivity of the antibodies changed during misfolding and self-assembly of SOD1 under reducing conditions. Because of the high variability in the ThT behavior under these conditions (Figure 1), and because the “pause” period, P_1 , was the time when the highest activity was observed for most of the antibodies, we divided the different aggregation reactions into two groups defined by the duration of

P_1 (t_{P_1}). Group 1 included reactions with a short P_1 , $t_{P_1} \leq 10$ h, comprising $\sim 75\%$ of the WT SOD1 reactions, and $t_{P_1} \leq 7$ h, comprising $\sim 50\%$ of the reactions of G93A-SOD1 (Figure 4). Group 2 comprised the remaining reactions with $t_{P_1} > 10$ h for WT SOD1 ($\sim 25\%$ of the reactions) and $t_{P_1} > 7$ h for G93A-SOD1 ($\sim 50\%$ of the reactions, Figure 5). In each figure, panels E and F show an example of one ThT profile, which were chosen with particularly short P_1 periods in Figure 4 and long P_1 periods in Figure 5 to demonstrate the high variability in kinetics. The dot-blot graphs in panels C and D are averages of multiple reactions and should not be compared directly to the single ThT examples.

Under these conditions, all the antibodies, except C4F6, showed an initial increase in reactivity with WT SOD1 followed by a decline. This change was statistically significant for the reactivity of all antibodies with WT SOD1 except for pAb 2770 (Figures 4C, 5C). AMF7-63 showed a statistically significant change in slow reactions (Figure 5C) but not fast reactions (Figure 4C). C4F6 did not react with WT SOD1, similar to the results under nonreducing conditions. Under these conditions, only the unreactive C4F6 and highly reactive 10C12 differed significantly from the other antibodies, whereas the reactivities of Ab16831, 2770, B8H10, AMF7-63, and 3H1 did not differ significantly from each other (Figures 4C, 5C).

In the case of G93A-SOD1, all the antibodies, including C4F6 showed a significant change in reactivity during the aggregation reaction (Figure 4D). The change was smaller for mAbs 3H1 and C4F6 than for other antibodies. 3H1 reached maximal reactivity at 12 h, later than most other antibodies, which showed maximal reactivity between 4–8 h (Figure 4D). C4F6 had its maximal reactivity between 0–4 h, and then the signal declined to about 50% of the original reactivity by 24 h and did not change at later time points. The ~ 2 -fold change in C4F6 was the smallest of all the antibodies tested, supporting the notion that it was specific for the apo form of G93A-SOD1 variant itself and was affected to a small degree by conformational change.

Comparison of antibody reactivities showed again three groups in the fast reactions (Figure 4D), which differed significantly from each other. These groups were a low-reactivity group comprising C4F6 and 3H1; a medium-reactivity group consisting of Ab16831, B8H10, and AMF7-63; and a high-reactivity group including 2770 and 10C12. In the medium-reactivity group, AMF7-63 deviated significantly from Ab16831 and B8H10 at later time points, in which its reactivity remained relatively high compared to the other two antibodies. In slow reactions (Figure 5D), the reactivity of most antibodies was somewhat higher than in the fast reactions, leading to a shift of antibodies Ab16831, B8H10, and AMF7-63 to the high reactivity group, and separation between C4F6, which remained the one with the lowest reactivity, and 3H1, which displayed medium reactivity (Figure 5D).

Interestingly, the reactivity of C4F6 with G93A-SOD1 under reducing conditions (Figures 4, 5) was $\leq 50\%$ of its reactivity under nonreducing conditions (Figure 3). Importantly, both conditions were blotted and developed on the same membranes allowing side-by-side comparison. These results suggested that the antibody recognizes an epitope containing A93 in the folded conformation of the protein and actually loses some of its reactivity when G93A-SOD1 misfolds and aggregates.

The reactivity of most of the other antibodies was substantially higher for G93A-SOD1 than for WT SOD1. The one exception was mAb 10C12, which showed high reactivity with both forms of SOD1. In the case of WT SOD1, the maximal

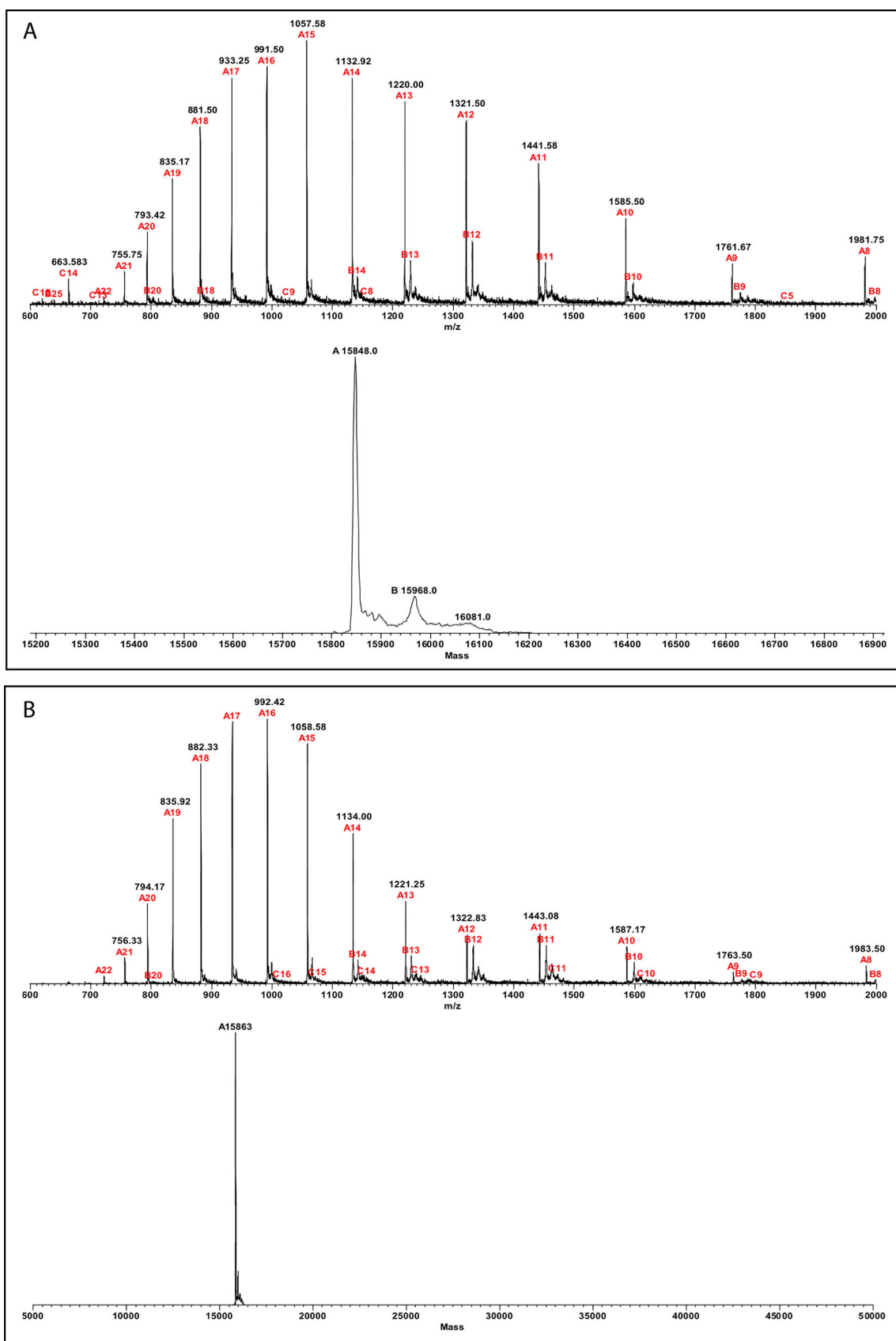


Figure 6. Mass-spectrometry characterization of WT and G93A-SOD1. Each protein was incubated in the presence of 0.25 M DTT for 10 min at RT and then subjected to LC-MS analysis. (A) Recorded (top) and deconvoluted (bottom) spectra of WT SOD1. (B) Recorded (top) and deconvoluted (bottom) spectra of G93A-SOD1. The fragmentation type (A, B, or C) and charge of each fragment is indicated in red and the observed mass in black.

Table 2. Reactivity of Different Antibodies with WT and G93A

antibody	metalated form reactivity ^a	reactivity at $t = 0$ h ^b	reactivity at $t = 4$ h ^b	maximal reactivity time (Figure 4/Figure 5)	maximal reactivity ^c	reactivity at $t = 40$ h ^{b,d}
WT-SOD1						
Ab16831	R	1086 ± 990	1651 ± 1595	8/12	2373 ± 1359	1288 ± 1228
2770	R	1596 ± 727	1980 ± 848	4/4 ^e	1980 ± 848	1336 ± 1195
B8H10	R	1384 ± 367	1973 ± 535	12/12 ^e	2032 ± 699	868 ± 843
C4F6	U	0 ± 0	0 ± 0		0 ± 0	
AMF7-63	R	993 ± 293	1672 ± 576	12/40	2316 ± 732	1985 ± 1408
3H1	U	547 ± 108	1188 ± 226	12/24	1834 ± 719	1286 ± 1022
10C12	U	1603 ± 438	4171 ± 1180	8/12	4929 ± 947	2502 ± 1804
G93A-SOD1						
Ab16831	R	2238 ± 909	3313 ± 817	12/16	4785 ± 1310	550 ± 171
2770	R	3472 ± 1189	4381 ± 1295	4/16	5182 ± 708	431 ± 347
B8H10	R	2570 ± 845	3166 ± 476	12/16	5285 ± 1636	797 ± 301
C4F6	U	1933 ± 333	1933 ± 166	4/8 ^e	2029 ± 319	1174 ± 664
AMF7-63	R	1779 ± 533	2740 ± 819	12/16	5164 ± 656	1664 ± 997
3H1	U	585 ± 177	1027 ± 259	12/20	3418 ± 1459	1829 ± 1920
10C12	U	3220 ± 803	4099 ± 701	4/8	4919 ± 393	478 ± 248

^aThe metalated form was analyzed separately from the apo form, and therefore, the two cannot be compared quantitatively. Therefore, we only indicate if the metalated form was reactive (R) or unreactive (U). ^bValues are average of the densitometry values shown in Figures 4C,D and 5C,D. ^cThe reactivity at the maximal time each in Figures 4 and 5 was averaged. ^dThe reactivity in fast reactions (Figure 4) was substantially lower than that of slow reactions (Figure 5). ^eThe antibody showed relatively little variation with time.

reactivity of 10C12, at $t = 8-12$ h, was 2–4 times higher than that of all other antibodies. As shown in Figure 5, this peak in reactivity corresponded approximately to the beginning of the P1 phase in the ThT curve. In reactions of WT SOD1 with a short P1 phase (Figure 4A,C), most of the antibodies also showed maximal reactivity around the same time, but their reactivity was substantially lower than that of 10C12. mAbs AMF7-63, 3H1, and 10C12 showed consistently a significant change in reactivity over the course of the aggregation reaction with WT SOD1, regardless of the kinetics of individual reactions. In contrast, the change was statistically significant for Ab16831 and B8H10 in reactions with a short P1 (Figure 4C), but not in those with a long P1 (Figure 5C). The reactivity of pAb 2770 did not change significantly during the aggregation of WT SOD1.

mAb 10C12 was raised against a form of the SOD1-exposed-dimer-interface (SEDI) antigen containing a cysteic acid residue,¹³ which raised the concern that it might have bound to an inadvertently oxidized form of SOD1. To test if this were the case, we examined the proteins by MS. These experiments were done in the presence of DTT to facilitate reduction of disulfide bonds. However, if cysteic acid existed in the protein, it could not have been reduced by DTT.³³ The observed masses of WT and G93A-SOD1, 15 848 and 15 863, respectively, corresponded to the intact polypeptides bound to two Na⁺ ions (calculated masses, 15 847 and 15 861, respectively). We did not observe oxidized forms of either WT or G93A-SOD1 in these experiments (Figure 6). To further test if a minor population of the protein contained cysteic acid, we incubated WT- or G93A-SOD1 with dimedone, a reagent used to label sulfenic acids. We did not detect a change in the molecular weight of either protein following incubation with dimedone (data not shown), suggesting that cysteic acid was not present in the proteins we used and did not contribute to mAb 10C12 binding. The reactivity of the antibody, thus, likely was against the unoxidized form of the SEDI region.

In the aggregation reactions of G93A-SOD1, all the antibodies showed significant changes in reactivity, regardless of kinetics (Figures 4D and 5D). In reactions with a short P1

phase, pAb 2770 behaved similarly to 10C12 (Figure 4B,D). Both antibodies had the highest reactivity for G93A-SOD1 and both displayed 5-times higher reactivity at ~ 8 h, approximately correlating with the P1 phase in the ThT curve, than at the end of the reaction. Reactions with longer P1 showed that the peak in reactivity of 10C12 actually was the earliest, at ~ 12 h, whereas the peak in reactivity of other antibodies was at 16–20 h and the latest one to peak was mAb 3H1 (Figure 5B,D). Interestingly, although the reactivity of all the antibodies started to decrease at ~ 12 h in reactions of G93A-SOD1 with a short P1 (Figure 4B,D) or $\sim 16-20$ h in reactions with a long P1 (Figure 5B,D), concomitantly with the second increase in ThT fluorescence (Figures 4E, 5F), the reactivity continued to decrease after the ThT fluorescence reached the final plateau, P2 (~ 16 h in Figure 4F and ~ 28 h in Figure 5F), suggesting that additional conformational changes and/or self-association took place during that period. These changes were not reflected in the ThT fluorescence, but possibly were associated with the morphological changes observed in Figure 2. Antibodies AMF7-63 and 3H1 were less sensitive to this change than the other antibodies, suggesting that the common antigen of these antibodies (Table 1) becomes only partially shielded at the time β -sheet-rich aggregates formed.

The observed reactivity of the antibodies with the different forms of SOD1 is summarized in Table 2. Taken together, the data suggested that of the three new antibodies, mAb 10C12 was the most sensitive for misfolded WT SOD1. Its sensitivity and selectivity exceeded not only those of the other new mAbs, 3H1 and AMF7-63, but also of the commercial mAb B8H10. In the case of G93A-SOD1, 10C12 showed similar sensitivity and selectivity for misfolded SOD1, with a preference for early forming oligomers. mAbs 3H1 and AMF7-63 also were sensitive and selective for misfolded G93A-SOD1. The peak in reactivity followed the order 10C12 (~ 12 h), AMF7-63 (~ 16 h), and finally 3H1 (~ 20 h, Figure 5D). However, as discussed above, the latter two antibodies had lower selectivity between oligomers and later forming β -sheet-rich aggregates than 10C12 or the commercial antibodies. These results suggest that at least three states can be distinguished by the panel of

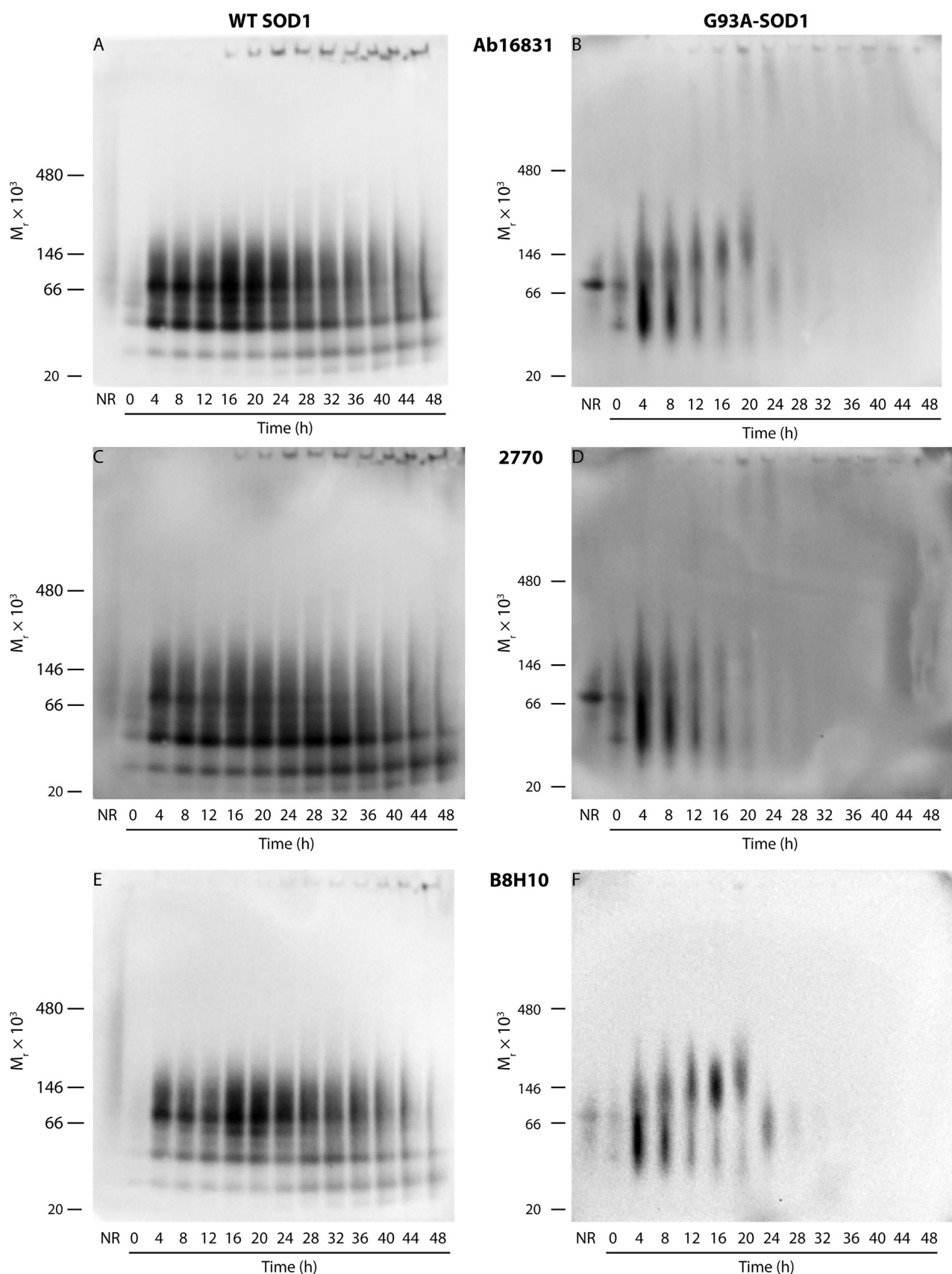


Figure 7. Native-PAGE/Western blot analysis of WT and G93A-SOD1 during aggregation. 40 μ M of WT (A, C, E) or G93A- (B, D, F) SOD1 were incubated at 37 $^{\circ}$ C with fast agitation in the presence of 25 mM DTT. Aliquots were taken every 4 h, flash frozen, and stored at -80° C. At the end of the reactions, the aliquots were fractionated by native PAGE, and the proteins were transferred to nitrocellulose membranes and probed with each antibody. Only Ab16831 (A,B), 2770 (C,D), and B8H10 yielded sufficient signal of signal-to-noise ratio and therefore the other antibodies are not shown. NR = nonreduced. Positions of molecular-weight markers are shown on the left of each membrane.

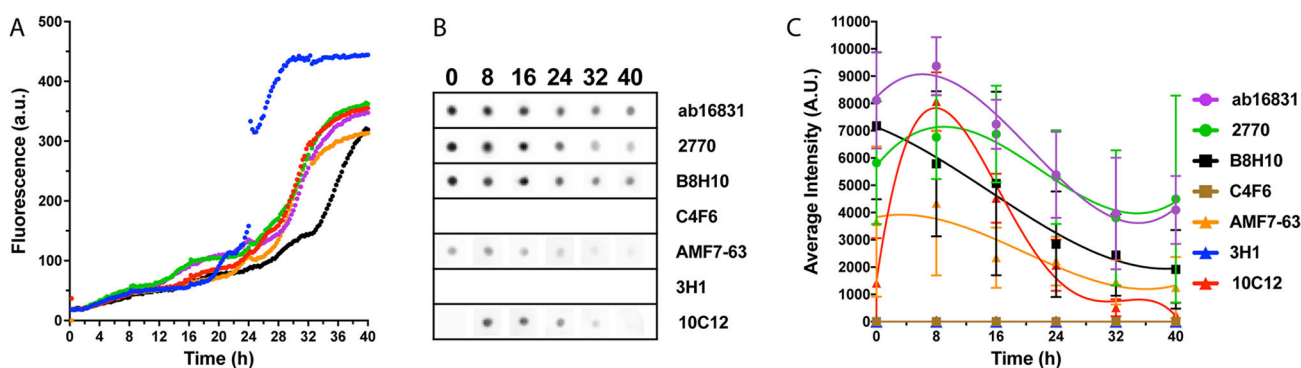


Figure 8. ThT fluorescence and antibody reactivity for E100K-SOD1. 40 μ M of E100 K-SOD1 were incubated at 37 $^{\circ}$ C with fast agitation in the presence of 25 mM DTT. (A) The change in ThT fluorescence was monitored in a plate reader for 40 h. (B) Representative dot blots with each antibody. (C) Averaged values from densitometric analysis of two independent experiments including a total of four replicates. The lines are added to help guide the eye but do not imply that the points should be connected.

antibodies we used—early, intermediate, and late oligomers. To our knowledge, these different oligomeric states are reported here for the first time. It will be highly interesting to attempt to isolate them and study the structural differences among them in the future.

The commercial antibody B8H10 behaved similarly to AMF7-63 during the aggregation reactions, showing moderate reactivity with little change over time for WT SOD1, but a strong sensitivity and selectivity for misfolded G93A-SOD1, with a peak at \sim 16 h and little reactivity for β -sheet-rich aggregates. As discussed above, antibody C4F6 bound only to G93A-SOD1 but showed little change in reactivity with misfolding or aggregation. A highly surprising result was the behavior of the polyclonal antibodies, Ab16831 and 2770 with G93A-SOD1. Both antibodies showed clear selectivity for the misfolded form of G93A-SOD1 protein, and little change in reactivity during the aggregation of WT SOD1, similar to B8H10, AMF7-63, and 3H1.

Characterization of the Reactivity of Anti-SOD1 Antibodies Using Native-PAGE/Western Blot. To gain further insight into the changes in SOD1 assembly state and the reactivity of the antibodies over time, we used native PAGE and Western blots. Aliquots of the reaction mixtures were fractionated by native PAGE, transferred to nitrocellulose membranes, and probed sequentially with the seven antibodies. As was done in the dot-blot experiments, the order of the antibodies was changed for each of three replicate membranes to avoid potential loss of signal during strip/reprobe cycles.

Interestingly, the new mAbs, AMF7-63, 3H1, and 10C12 showed no reactivity at all in the Western blot experiments. The two pAbs, Ab16831 and 2770, reacted with both WT SOD1 and G93A-SOD1 and revealed changes in assembly state over time (Figure 7). mAb B8H10 showed a similar reactivity pattern to the two pAbs, whereas C4F6 had very weak reactivity with G93A-SOD1 only (data not shown). Ab16831, 2770, and B8H10 had a similar staining pattern and all three antibodies showed marked differences between WT SOD1 and G93A-SOD1.

Interestingly, these three antibodies had low reactivity with nonreduced (NR) WT SOD1 or with reduced SOD1 at $t = 0$ h, whereas at the next time point, $t = 4$ h, the reactivity increased substantially. The blots showed two main bands, likely corresponding to native SOD1 dimer and to the monomer generated by its dissociation. The mobilities of these bands corresponded to higher molecular weights than those of SOD1

monomer and dimer (calculated MW = 15.8 and 31.6 kDa, respectively), which is typical for native PAGE. Additional bands between the monomer and dimer and below the monomer presumably corresponded to minor alternative conformations or degradation products. The intensity of the dimer band appeared to reach a maximum at 16 h when probing with Ab16831 (Figure 7A) and B8H10 (Figure 7E), but not when probing with 2770 (Figure 7C). At later time points, the intensity of both bands decreased gradually. The dimer band decreased more rapidly, consistent with its dissociation into monomers. Starting at $t = 20$, high-molecular-weight protein, which did not enter the gel, was observed at the bottom of the wells, suggesting formation of aggregates, in agreement with the ThT (Figure 1C) and EM (Figure 2) data. Concomitant with these changes, the intensity of the two bands with the fastest mobility increased gradually. We believe that these bands may be alternative conformations of monomeric SOD1. We cannot rule out that they were degradation products, but their recognition by B8H10 suggests against this interpretation.

The pattern observed with G93A-SOD1 was distinct. A strong dimer bands was observed in the NR lane with Ab16831 (Figure 7B) and 2770 (Figure 7D), and a monomer band appeared immediately following addition of DTT at $t = 0$ h. These bands also were detected by B8H10, but their reactivity with this antibody was much weaker, in agreement with its characterization as selective for misfolded SOD1. At 4 h, a high-intensity smeary band appeared, likely corresponding to multiple conformers of the monomer, and a higher molecular weight smear was observed above it, presumably representing G93A-SOD1 dimer, trimer, and possibly higher-molecular-weight oligomers. With time, the lower band's intensity decreased and the higher band's intensity increased, consistent with their assignment as monomer and oligomers, respectively. Probing with Ab16831 (Figure 7B) or B8H10 (Figure 7F), but not 2770 (Figure 7D), revealed that between 12–20 h, the apparent molecular weight of the smeary oligomer band increased somewhat. At the same time, high-molecular-weight putative protein aggregates at the bottom of the well were observed in blots probed by Ab16831 or 2770, but not B8H10.

Overall, the native-PAGE/Western-blot data demonstrated different behaviors of WT- and G93A-SOD1. As expected, the disease-associated variant converted into putative insoluble, high-molecular-weight aggregates substantially faster than the WT protein and the G93A-SOD1 intermediates forming along the way were smeerier and less distinct than those of WT SOD1.

Presumably, although native PAGE is a mild, nondenaturing electrophoretic method, unlike dot blots, it is sufficient to induce conformational changes precluding recognition of any form of SOD1 by AMF7-63, 3H1, and 10C12, and to a large extent also of G93A-SOD1 by C4F6.

Examination of E100 K-SOD1 by Dot Blots. In view of the surprising behavior of the antibodies, we asked if the pattern of the reactivity against mutant SOD1 was specific for the G93A variant. To address this question, we tested the reactivity of the antibodies using the dot-blot paradigm against a variant containing an amino-acid substitution close to G93A—E100K-SOD1. In this case, dot-blots were obtained every 8 h, rather than 4 h, but other aspects of the experiment were similar. Six replicate reactions were analyzed, showing a similar behavior to G93A-SOD1 (Figure 8A). The lower absolute ThT fluorescence levels in experiments with E100 K-SOD1 (cf. Figure 1D and 8A) were due to different instrument settings. Four of the reactions (green, red, purple, and orange curves in Figure 8A) followed highly similar courses, and therefore, the quantitative dot-blot analysis included only these four reactions. The behavior of most antibodies toward E100K-SOD1 was similar to their reactivity with WT SOD1 (Figure 8B,C). Thus, Ab16831, 2770, and B8H10 showed relatively high reactivity already at $t = 0$, and their reactivity decreased by up to 2-fold with aggregation. AMF7-63 showed a similar pattern but had lower reactivity toward E100K-SOD1 than the former three antibodies. Antibody 10C12 showed no reactivity at $t = 0$, but a strong reactivity peak at $t = 8$, followed by a sharp decline in reactivity at later time points. Surprisingly, 3H1 behaved similarly to C4F6 in this case and showed no reactivity with E100K-SOD1 regardless of aggregation. These observations supported the notion that C4F6 was specific for G93A-SOD1 and not for a misfolded form of the protein and suggested that despite being raised against the same peptide epitope, SOD1(125–142), antibodies 3H1 and AMF7-63 differ not only in reactivity but also in the actual three-dimensional epitope they bind to.

Another surprising finding was that the commercial mAbs, B8H10 and C4F6 had different selectivity profiles than those previously reported.^{27–29,31,32} Although B8H10 showed a peak in reactivity followed by a decline during the aggregation of SOD1, which was more prominent in the case of the G93A and E100K variants (Figure 4, 5, 8) than the WT protein, this mAb also showed high reactivity with unaggregated SOD1 incubated under nonreducing conditions (Figure 3). This kind of behavior was expected, and indeed was confirmed, for Ab16831 and 2770, but not for B8H10. Nonetheless, the mAb reacted with WT SOD1 under nonreducing conditions at the same level as the two pAbs (Figure 3A,C). In the case of G93A-SOD1, the reactivity of B8H10 under nonreducing conditions was similar to that of Ab16831, whereas 2770 showed higher reactivity (Figure 3B,D). These three antibodies actually showed lower reactivity for WT SOD1 under reducing conditions than under nonreducing conditions (cf. Figure 3 with Figures 4, 5). Taken together, the data suggest that mAb B8H10 reacts with both folded and misfolded SOD1 and is not more specific for misfolded SOD1 than antibodies Ab16831 or 2770.

The most surprising behavior was of antibody C4F6, which showed no reactivity with WT or E100K-SOD1 regardless of folding/misfolding, strong reactivity with apoG93A-SOD1 under nonreducing conditions (the strongest of the seven antibodies tested), weaker reactivity under reducing conditions, and little change with oligomerization and aggregation (Figures

3–5, 8). C4F6 did not react with metalated G93A-SOD1 (Figure 3B). Thus, our data suggest that this antibody is specific for an epitope in G93A-SOD1 that does not exist in WT or E100K-SOD1, is obscured in the metal-bound form of this variant, and is partially shielded under reducing conditions, regardless of misfolding or self-assembly of G93A-SOD1.

In summary, by monitoring the aggregation of WT and disease-associated SOD1 forms using ThT fluorescence, EM, dot blots, and native-PAGE/Western blots with seven different antibodies, we provide evidence for the existence of at least three intermediate structures that form and disappear during the self-assembly process of the protein under reducing conditions. Distinction of these intermediates has not been reported previously and may lead to identification of potential targets for therapeutic intervention. In addition, our data indicate that currently used commercial antibodies have different specificity and selectivity profiles than previously reported and interpretation of data obtained using these antibodies should be exercised with caution.

METHODS

Protein Expression and Purification. Human, WT, G93A-, and E100K-SOD1 were expressed in *Saccharomyces cerevisiae* and purified by sequential chromatography according to published protocols.³⁴ Part of each protein preparation was demetalated using EDTA by dialysis as described previously.^{5,34} Metalated and demetalated proteins were flash-frozen in liquid nitrogen and stored at -80°C .

ThT Fluorescence Assay. Reaction mixtures containing 10 mM potassium phosphate, 40 μM WT, G93A-, or E100K-SOD1 were prepared in the absence (WT and G93A-SOD1 only) or presence (all three isoforms) of 25 mM DTT. All solutions were made freshly and filtered through 0.2- μm filters. The reactions were conducted in two formats: For comparison between ThT fluorescence and dot blots (Figures 1, 3–5, and 8) the reactions were carried out in white Nunc 96-Well Optical-Bottom plates with a polymer base (Thermo Fisher), which were agitated using an elliptical motion at 1,020 rpm. Each well contained 40 μM ThT and fluorescence was monitored every 15 min in a BioTek Synergy HT Multi-Detection Microplate Reader at $\lambda_{\text{ex}} = 420$ nm (slit width = 50 nm) and $\lambda_{\text{em}} = 485$ nm (slit width = 20 nm). For comparison with electron microscopy (EM, Figure 2, WT and G93A-SOD1 only), reactions were performed in the absence of ThT because control reactions containing no protein showed ThT crystals on the EM grids. 1-mL reaction mixtures containing 40 μM WT or G93A-SOD1 in the absence or presence of 25 mM DTT were incubated at 37°C with agitation at 300 rpm. To monitor the SOD1 aggregation, 40 μL of the reaction mixtures were mixed with 260 μL of 120 μM ThT at 4 h intervals and the fluorescence was measured using a F-4500 Fluorescence Spectrophotometer at $\lambda_{\text{ex}} = 450$ nm (slit width = 5 nm) and $\lambda_{\text{em}} = 485$ nm (slit width = 10 nm).

Electron Microscopy. Aliquots (10 μL) from the ThT reactions in the second format were applied to glow-discharged, carbon-coated Formvar grids (Electron Microscopy Sciences, FCF400-CU) as described previously^{35,36} and incubated for 2 min. The solution was wicked off gently using Whatman, grade-2 filter paper. The proteins were stained with 10 μL of 1% uranyl acetate (Ted Pella, Inc.) for 2 min and wicked dry using filter paper. The grid was washed three times with deionized water at 2 min intervals, the solutions were wicked off, and the grids were air-dried. The samples were examined using a JEOL 1200 electron microscope operating at 80 keV.

Dot Blot. Aliquots (2 μL) of each reaction mixture were taken every 4 h (WT and G93A-SOD1) or every 8 h (E100K-SOD1) during the aggregation reactions and loaded onto nitrocellulose membranes. Two independent experiments were conducted with six replicates each of reducing (all three variants) and nonreducing (WT and G93A-SOD1 only) conditions. The metalated proteins (WT and G93A-SOD1 only) were probed without incubation as a control in separate dot-blots. The membranes were incubated in ~ 10 mL of blocking buffer containing

5% nonfat, dry-milk powder in 20 mM Tris HCl, 150 mM NaCl, 0.1% Tween-20, pH 7.4 (TBST), with mild agitation for 1 h at RT or overnight at 4 °C. Then, the membranes were incubated with 10 mL solutions of each primary antibody in blocking buffer overnight at 4 °C. The following commercial antibodies and dilutions were used: Ab16831 (Abcam, 1:2,000), 2770 (Cell Signaling Technology, 1:1,000), B8H10 (MédiMabs, 1:500), and C4F6 (MédiMabs, 1:500). Additionally, the following new antimisfolded SOD1 antibodies and dilutions were used: AMF7-63 (1:500), 10C12 (1:500), and 3H1 (1:500).

The membranes were washed with blocking buffer twice for 5 min and then incubated with 10 mL of horseradish peroxidase-conjugated goat antirabbit secondary antibody (Santa Cruz Biotechnology, 1:2000 dilution) or horse antimouse secondary antibody (Cell Signaling Technology, 1:2000), as appropriate, for 2 h at RT with mild agitation and washed twice with 10 mL of TBST for 10 min. Finally, the dots were visualized using a HyGLO Quick Spray chemiluminescence kit (Denville Scientific). Images were captured using a Syngene multi-application gel imaging system PXi and quantified using ImageJ.³⁷ After image visualization, the membranes were rehydrated and stripped of antibodies using a Blot Restore Membrane Rejuvenation Kit (Millipore Sigma). The membranes then were reprobed with the next antibody. This process was repeated to analyze multiple antibodies using the same membranes.

Native-PAGE/Western blot. Two μg protein per sample from each time point were fractionated using NuPage 4–16% Bis-Tris gels in triplicates and the proteins were transferred to 0.2- μm pore size nitrocellulose membranes. Membranes were probed using the seven antibodies in the following dilutions: Ab16831, 1:2000; 2770, 1:1000; B8H10, 1:500; C4F6, 1:500; AMF7-63, 1:500; 3H1, 1:500; and 10C12, 1:500. HRP-conjugated secondary antimouse or antirabbit antibodies were used at 1:10 000 and 1:2000 dilutions, respectively, and bands were visualized using HyGLO Quick Spray chemiluminescence detection reagent (Denville, #E2400) and imaged using a Syngene PXi digital imager (Syngene, Frederick, MD). After imaging, the antibodies were stripped using Restore Plus Western blot stripping buffer (Thermo Scientific), and then the blots were reprobed using a different order of antibodies for each replicate.

LC-MS. A 3- μL solution of WT or G93A-SOD1 was incubated in the presence of 0.25 M DTT for 10 min at RT, mixed with 7 μL of formic acid and fractionated into a ThermoFisher LTQ XL mass spectrometer via a 2 mm SW2000 capillary column using a 4:4:1 mixture of chloroform/methanol/1% formic acid. Mass spectra were recorded in a positive-ion mode. Spectra were deconvoluted using MagTran.

■ ASSOCIATED CONTENT

● Supporting Information

The Supporting Information is available free of charge on the ACS Publications website at DOI: 10.1021/acschembio.8b00729.

Supplementary Figure 1: Comparison of SOD1 aggregation under different conditions (PDF)

■ AUTHOR INFORMATION

Corresponding Author

*E-mail: gbitan@mednet.ucla.edu. Tel. (310) 206-2082. Fax. (310) 206-1700.

ORCID

Gal Bitan: 0000-0001-7046-3754

Notes

The authors declare the following competing financial interest(s): NC serves as a Chief Scientific Officer of ProMIS Neurosciences, which holds a license for commercial development of antibodies AMF 7-63, 3H1, and 10C12. All other authors declare that they have no conflicts of interest with the contents of this article.

■ ACKNOWLEDGMENTS

We thank J. Valentine for the generous gift of yeast cell lines expressing WT, G93A-, and E100K-SOD1. The work was supported by RGK Foundation grant 20143057.

■ REFERENCES

- (1) Gordon, P. H. (2011) Amyotrophic lateral sclerosis: pathophysiology, diagnosis and management. *CNS Drugs* 25, 1–15.
- (2) Nedd, S., Redler, R. L., Proctor, E. A., Dokholyan, N. V., and Alexandrova, A. N. (2014) Cu,Zn-superoxide dismutase without Zn is folded but catalytically inactive. *J. Mol. Biol.* 426, 4112–4124.
- (3) Toichi, K., Yamanaka, K., and Furukawa, Y. (2013) Disulfide scrambling describes the oligomer formation of superoxide dismutase (SOD1) proteins in the familial form of amyotrophic lateral sclerosis. *J. Biol. Chem.* 288, 4970–4980.
- (4) Leal, S. S., Cristovao, J. S., Bieseimer, A., Cardoso, I., and Gomes, C. M. (2015) Aberrant zinc binding to immature conformers of metal-free copper-zinc superoxide dismutase triggers amorphous aggregation. *Metallomics* 7, 333–346.
- (5) Chattopadhyay, M., Durazo, A., Sohn, S. H., Strong, C. D., Gralla, E. B., Whitelegge, J. P., and Valentine, J. S. (2008) Initiation and elongation in fibrillation of ALS-linked superoxide dismutase. *Proc. Natl. Acad. Sci. U. S. A.* 105, 18663–18668.
- (6) Banerjee, V., Shani, T., Katzman, B., Vyazmensky, M., Papo, N., Israelson, A., and Engel, S. (2016) Superoxide Dismutase 1 (SOD1)-Derived Peptide Inhibits Amyloid Aggregation of Familial Amyotrophic Lateral Sclerosis SOD1 Mutants. *ACS Chem. Neurosci.* 7, 1595–1606.
- (7) Ivanova, M. I., Sievers, S. A., Guenther, E. L., Johnson, L. M., Winkler, D. D., Galaledeen, A., Sawaya, M. R., Hart, P. J., and Eisenberg, D. S. (2014) Aggregation-triggering segments of SOD1 fibril formation support a common pathway for familial and sporadic ALS. *Proc. Natl. Acad. Sci. U. S. A.* 111, 197–201.
- (8) Kaye, R., Head, E., Thompson, J. L., McIntire, T. M., Milton, S. C., Cotman, C. W., and Glabe, C. G. (2003) Common structure of soluble amyloid oligomers implies common mechanism of pathogenesis. *Science* 300, 486–489.
- (9) Gerson, J. E., Sengupta, U., Lasagna-Reeves, C. A., Guerrero-Munoz, M. J., Troncoso, J., and Kaye, R. (2014) Characterization of tau oligomeric seeds in progressive supranuclear palsy. *Acta Neuropathol. Commun.* 2, 73.
- (10) Glabe, C. G. (2008) Structural classification of toxic amyloid oligomers. *J. Biol. Chem.* 283, 29639–29643.
- (11) Hatami, A., Albay, R., 3rd, Monjazeb, S., Milton, S., and Glabe, C. (2014) Monoclonal antibodies against A β 42 fibrils distinguish multiple aggregation state polymorphisms in vitro and in Alzheimer disease brain. *J. Biol. Chem.* 289, 32131–32143.
- (12) Hatami, A., Monjazeb, S., and Glabe, C. (2016) The Anti-Amyloid- β Monoclonal Antibody 4G8 Recognizes a Generic Sequence-Independent Epitope Associated with α -Synuclein and Islet Amyloid Polypeptide Amyloid Fibrils. *J. Alzheimer's Dis.* 50, S17–S25.
- (13) Rakhit, R., Robertson, J., Vande Velde, C., Horne, P., Ruth, D. M., Griffin, J., Cleveland, D. W., Cashman, N. R., and Chakrabartty, A. (2007) An immunological epitope selective for pathological monomer-misfolded SOD1 in ALS. *Nat. Med.* 13, 754–759.
- (14) Baker, M. (2015) Antibody anarchy: A call to order. *Nature* 527, S45–S51.
- (15) Bradbury, A., and Pluckthun, A. (2015) Reproducibility: Standardize antibodies used in research. *Nature* 518, 27–29.
- (16) Baker, M. (2015) Reproducibility crisis: Blame it on the antibodies. *Nature* 521, 274–276.
- (17) Grad, L. L., Yerbury, J. J., Turner, B. J., Guest, W. C., Pokrishevsky, E., O'Neill, M. A., Yanai, A., Silverman, J. M., Zineddine, R., Corcoran, L., Kumita, J. R., Luheshi, L. M., Yousefi, M., Coleman, B. M., Hill, A. F., Plotkin, S. S., Mackenzie, I. R., and Cashman, N. R. (2014) Intercellular propagated misfolding of wild-type Cu/Zn superoxide dismutase occurs via exosome-dependent and -independent mechanisms. *Proc. Natl. Acad. Sci. U. S. A.* 111, 3620–3625.

- (18) LeVine, H., 3rd. (1999) Quantification of β -sheet amyloid fibril structures with thioflavin T. *Methods Enzymol.* 309, 274–284.
- (19) Abdolvahabi, A., Shi, Y., Chuprin, A., Rasouli, S., and Shaw, B. F. (2016) Stochastic Formation of Fibrillar and Amorphous Superoxide Dismutase Oligomers Linked to Amyotrophic Lateral Sclerosis. *ACS Chem. Neurosci.* 7, 799–810.
- (20) Abdolvahabi, A., Shi, Y., Rasouli, S., Croom, C. M., Aliyan, A., Marti, A. A., and Shaw, B. F. (2017) Kaplan-Meier Meets Chemical Kinetics: Intrinsic Rate of SOD1 Amyloidogenesis Decreased by Subset of ALS Mutations and Cannot Fully Explain Age of Disease Onset. *ACS Chem. Neurosci.* 8, 1378–1389.
- (21) Lang, L., Zetterstrom, P., Brannstrom, T., Marklund, S. L., Danielsson, J., and Oliveberg, M. (2015) SOD1 aggregation in ALS mice shows simplistic test tube behavior. *Proc. Natl. Acad. Sci. U. S. A.* 112, 9878–9883.
- (22) Shi, Y., Rhodes, N. R., Abdolvahabi, A., Kohn, T., Cook, N. P., Marti, A. A., and Shaw, B. F. (2013) Deamidation of asparagine to aspartate destabilizes Cu, Zn superoxide dismutase, accelerates fibrillization, and mirrors ALS-linked mutations. *J. Am. Chem. Soc.* 135, 15897–15908.
- (23) Oztug Durer, Z. A., Cohlberg, J. A., Dinh, P., Padua, S., Ehrenclou, K., Downes, S., Tan, J. K., Nakano, Y., Bowman, C. J., Hoskins, J. L., Kwon, C., Mason, A. Z., Rodriguez, J. A., Doucette, P. A., Shaw, B. F., and Valentine, J. S. (2009) Loss of metal ions, disulfide reduction and mutations related to familial ALS promote formation of amyloid-like aggregates from superoxide dismutase. *PLoS One* 4, e5004.
- (24) Banci, L., Bertini, I., Boca, M., Giroto, S., Martinelli, M., Valentine, J. S., and Vieru, M. (2008) SOD1 and amyotrophic lateral sclerosis: mutations and oligomerization. *PLoS One* 3, e1677.
- (25) Nilsson, M. I., Macneil, L. G., Kitaoka, Y., Alqarni, F., Suri, R., Akhtar, M., Haikalas, M. E., Dhaliwal, P., Saeed, M., and Tarnopolsky, M. A. (2014) Redox state and mitochondrial respiratory chain function in skeletal muscle of LGMD2A patients. *PLoS One* 9, e102549.
- (26) Thompson, M. L., Chen, P., Yan, X., Kim, H., Borom, A. R., Roberts, N. B., Caldwell, K. A., and Caldwell, G. A. (2014) TorsinA rescues ER-associated stress and locomotive defects in *C. elegans* models of ALS. *Dis. Models & Mech.* 7, 233–243.
- (27) Roberts, B. R., Lim, N. K., McAllum, E. J., Donnelly, P. S., Hare, D. J., Doble, P. A., Turner, B. J., Price, K. A., Chun Lim, S., Paterson, B. M., Hickey, J. L., Rhoads, T. W., Williams, J. R., Kanninen, K. M., Hung, L. W., Liddell, J. R., Grubman, A., Monty, J. F., Llanos, R. M., Kramer, D. R., Mercer, J. F., Bush, A. I., Masters, C. L., Duce, J. A., Li, Q. X., Beckman, J. S., Barnham, K. J., White, A. R., and Crouch, P. J. (2014) Oral treatment with Cu(II)(atsm) increases mutant SOD1 in vivo but protects motor neurons and improves the phenotype of a transgenic mouse model of amyotrophic lateral sclerosis. *J. Neurosci.* 34, 8021–8031.
- (28) Pickles, S., Semmler, S., Broom, H. R., Destroismaisons, L., Legroux, L., Arbour, N., Meiering, E., Cashman, N. R., and Vande Velde, C. (2016) ALS-linked misfolded SOD1 species have divergent impacts on mitochondria. *Acta Neuropathol. Commun.* 4, 43.
- (29) Patel, P., Kriz, J., Gravel, M., Soucy, G., Bareil, C., Gravel, C., and Julien, J. P. (2014) Adeno-associated virus-mediated delivery of a recombinant single-chain antibody against misfolded superoxide dismutase for treatment of amyotrophic lateral sclerosis. *Mol. Ther.* 22, 498–510.
- (30) Pokrishevsky, E., Grad, L. I., and Cashman, N. R. (2016) TDP-43 or FUS-induced misfolded human wild-type SOD1 can propagate intercellularly in a prion-like fashion. *Sci. Rep.* 6, 22155.
- (31) Bosco, D. A., Morfini, G., Karabacak, N. M., Song, Y., Gros-Louis, F., Pasinelli, P., Goolsby, H., Fontaine, B. A., Lemay, N., McKenna-Yasek, D., Frosch, M. P., Agar, J. N., Julien, J. P., Brady, S. T., and Brown, R. H., Jr. (2010) Wild-type and mutant SOD1 share an aberrant conformation and a common pathogenic pathway in ALS. *Nat. Neurosci.* 13, 1396–1403.
- (32) Ayers, J. I., Xu, G., Pletnikova, O., Troncoso, J. C., Hart, P. J., and Borchelt, D. R. (2014) Conformational specificity of the C4F6 SOD1 antibody; low frequency of reactivity in sporadic ALS cases. *Acta Neuropathol. Commun.* 2, 55.
- (33) Hamann, M., Zhang, T., Hendrich, S., and Thomas, J. A. (2002) Quantitation of protein sulfenic and sulfonic acid, irreversibly oxidized protein cysteine sites in cellular proteins. *Methods Enzymol.* 348, 146–156.
- (34) Doucette, P. A., Whitson, L. J., Cao, X., Schirf, V., Demeler, B., Valentine, J. S., Hansen, J. C., and Hart, P. J. (2004) Dissociation of human copper-zinc superoxide dismutase dimers using chaotrope and reductant. Insights into the molecular basis for dimer stability. *J. Biol. Chem.* 279, 54558–54566.
- (35) Lopes, D. H., Attar, A., Nair, G., Hayden, E. Y., Du, Z., McDaniel, K., Dutt, S., Bandmann, H., Bravo-Rodriguez, K., Mittal, S., Klärner, F. G., Wang, C., Sanchez-Garcia, E., Schrader, T., and Bitan, G. (2015) Molecular tweezers inhibit islet amyloid polypeptide assembly and toxicity by a new mechanism. *ACS Chem. Biol.* 10, 1555–1569.
- (36) Bitan, G., Tarus, B., Vollers, S. S., Lashuel, H. A., Condrion, M. M., Straub, J. E., and Teplow, D. B. (2003) A molecular switch in amyloid assembly: Met³⁵ and amyloid β -protein oligomerization. *J. Am. Chem. Soc.* 125, 15359–15365.
- (37) Abramoff, M. D., Magelhaes, P. J., and Ram, S. J. (2004) Image Processing with ImageJ. *Microsc. Microanal.* 11, 36–42.